 doi:10.20944/preprints202009.0381.v1

Article

Automated conditional screening of Escherichia coli knockout mutants in parallel adaptive fed-batch cultivations

Sebastian Hans [1*], Benjamin Haby [1], Niels Krausch [1], Tilman Barz [2], Peter Neubauer [1] and Mariano Nicolas Cruz-Bournazou[3]

[1] Technische Universität Berlin, Faculty III Process Sciences, Institute of Biotechnology, Chair of Bioprocess Engineering, Ackerstraße 76, 13357 Berlin, Germany; peter.neubauer@tu-berlin.de
[2] AIT Austrian Institute of Technology, Center for Energy; tilman.barz@ait.ac.at
[3] DataHow AG, ETH Zürich-HCI, F137, Vladimir-Prelog-Weg 1, 8093 Zurich, Switzerland; n.cruz@datahow.ch
* Correspondence: sebastian.hans@tu-berlin.de

Abstract: In bioprocess development, the host and the genetic construct for a new biomanufacturing process are selected in the early developmental stages. This decision, made at the screening scale with very limited information about the performance of the selected cell factory in larger reactors, has a major influence on the performance of the final process. To overcome this, scale-down approaches are essential to run screenings that show the real cell factory performance at industrial like conditions. We present a fully automated robotic facility with 24 parallel mini-bioreactors that is operated by a model based adaptive input design framework for the characterization of clone libraries under scale-down conditions. The cultivation operation strategies are computed and continuously refined based on a macro-kinetic growth model that is continuously re-fitted to the available experimental data. The added value of the approach is demonstrated with 24 parallel fed-batch cultivations in a mini-bioreactor system with eight different *Escherichia coli* strains in triplicate. The 24 fed-batches ran under the desired conditions generating sufficient information to define the fastest growing strain in an environment with varying glucose concentrations similar to industrial scale bioreactors.

Keywords: high throughput screening, rapid phenotyping, model-based experimental design, *Escherichia coli*, automated bioprocess development

1. Introduction

Emerging technologies in robotic biolaboratories open new opportunities for both, High Throughput (HT) Screening and HT Bioprocess Development. Screening can be roughly divided into two stages; (i) the "clone library screening" (10^6-10^{12} candidates/factors), with yes/no experiments in Micro Well Plates (MWP) [1–3], and (ii) the stage known as "conditional screening" [4–6], the focus of this work. During the "conditional screening" a reduced number of candidate strains is tested with factors that significantly influence the performance at industrial scale (e.g. media, pH and temperature profiles, bioreactor heterogeneities, induction and feeding strategies [7–12]). These factors are known to affect the underlying nonlinear dynamics of the bioprocess and are part of the very complex time-dependent interaction between the bioreactor environment and the cell factory. This highly nonlinear behavior makes it difficult to predict the effect of changes in the cultivating conditions and is responsible for the high failure rate in scale-up [13,14]. In order to overcome these challenges, experiments in conditional screening require highly advanced experimental setups able to: (i) operate as similar as possible to the industrial strategy (e.g. fed-batch or continuous cultivations), (ii) mimic the harsh conditions of industrial scale bioreactors as close as possible (e.g.

 doi:10.20944/preprints202009.0381.v1

growth limitation; bioreactor heterogeneities), and (iii) generate the maximal amount of information possible about the strain´s phenotype and its complex dynamic interaction with the process.

The technology to perform parallel experiments with advanced operation in fed-batch or continuous mode has recently become available [4,15,16]. Mini-BioReactors (MBR) integrated in Liquid Handling Stations (LHS) allow a large number of parallel cultivations while maintaining the properties of benchtop bioreactors. With working volumes of 2-250 mL [17], geometric similarities to large-scale reactors [18], and high frequency measurements and analytics, MBRs have been used for process characterizations [15,19–21] and scale-down studies [11,22] for up to 48 cultivations in parallel [23]. Such robotic facilities with automated cultivation control, sampling and at-line analytic operations [16,24] are very powerful systems that can accelerate bioprocess development, especially in combination with digital solutions for experiment planning [25–28], data acquisition [4,16]and real-time dynamic analysis [29,30]. The bottleneck is currently the lack of advanced computer aided tools to plan the experiments, operate the robots and build the necessary models and digital twins for scale-up and advanced process control. Because of limitations by the planning and operation capacity of humans much too often robots are on hold waiting for the next experiment to be planed, experimental campaigns need to be repeated because of failures that were not detected on time, and the same feeding strategy is used for strains with different characteristics . These are the main issues we address in the present work.

Initial attempts to solve these challenges have demonstrated the added value of model-based tools in terms of accelerating the development process and increasing robustness during scale-up [10,31,32]. Nevertheless, the existing solutions are mostly limited to single strain applications due to the complexity of the used mechanistic models and the difficulty to identify the parameters for a large number of strains at the same time [32,33]. Therefore, screening approaches often use simple black-box models for the microorganisms, which do not allow a detailed comparison of their phenotypes. This contribution proposes an advanced conditional screening design framework that can interact with the robotic facility to run fed-batch like cultivations with feeding strategies tailored for each strain. To achieve this, (i) a model with a general macro-kinetic structure is defined with model-parameter ranges that can describe the phenotypes of all strains, and (ii) a parameter estimation is carried out for each strain to obtain a characteristic parameter set that uniquely describes it. By this we gain not only a robust and accurate prediction of the characteristics of each strain, but we also can easily quantify and confidently compare their performance. Finally, the method is applied in an online model calibration framework to adaptively define individual optimal feed start and feeding strategy. The framework provides all necessary parameters and actions to define a wide range of alternative event triggers (e.g. depletion of glucose or consumption of acetate).

In summary, during the parallel cultivation the adaptive framework for conditional screening experiments recursively executes the following steps: (i) collection of cultivation data from the database, (ii) selection of an identifiable parameter (sub)set (PE regularization) for each strain, (iii) estimation of kinetic parameters for each clone, (iv) updating of the optimal feeding profiles for each clone, and (v) transfer of the new feeding profiles to the database (Figure 1). As a proof of concept, parallel screening experiments with eight different strains including six knockout mutants of *E. coli* K-12 are conducted in 24 mini bioreactors. At the start of the experiment, virtually no information on the growth behaviour of all these strains was available. In this one experiment it was possible to identify 13 model parameters for all clones with sufficient accuracy.

Preprints (www.preprints.org) | NOT PEER-REVIEWED | Posted: 17 September 2020 doi:10.20944/preprints202009.0381.v1

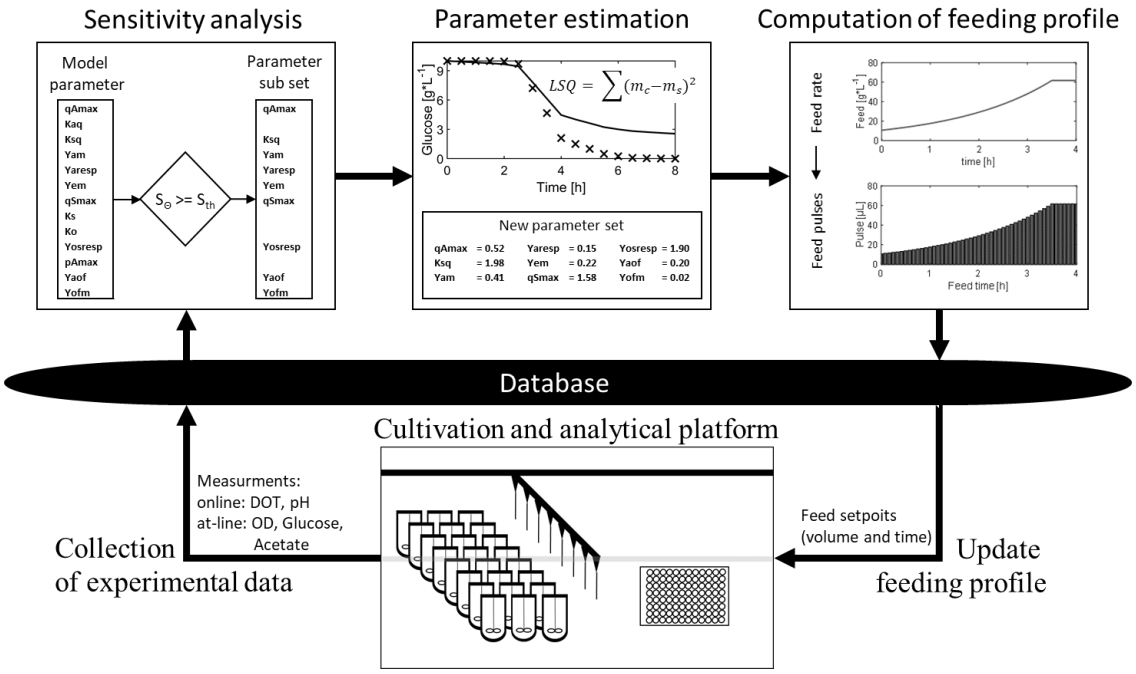

Figure 1: Illustration of the model calibration cycle in the adaptive framework for conditional screening experiments. On the *Cultivation and analysis platform* (consisting of two liquid handling stations, a mini-bioreactor system) the cultivation of the clones is performed, samples are collected and autonomously analyzed. The generated online and at-line measurements are sent to the central data storage (*database*). The model calibration cycle starts with the collection of all available data. Based on the measurements the *Sensitivity analysis* is performed, based on the results, the identifiable parameters are selected, and non-identifiable parameters are not considered/ fixed in the subsequent parameter estimation. In the *Parameter estimation*, the identifiable parameter subset is adjusted to fit the model to the measurements. Based on the calibrated model, in the *Feed calculation*, the feed is calculated according to previously defined criteria and further converted into corresponding pulses with individual times. These time/pulse setpoints are stored in the *Database* and executed directly by the *Cultivation and analysis platform*.

2. Materials and Methods

2.1. HTBD facility

The high throughput bioprocess development facility is composed of two liquid handling stations (Freedom Evo 200, Tecan, Switzerland; Microlab Star, Hamilton, Switzerland) and a mini-bioreactor system (48 BioReactor, 2mag AG, Munich, Germany). Both liquid handling stations are connected on hardware and software level to exchange samples, process and measurement information. A detailed description of the used hardware and software framework is given in Haby et al. 2019 [16].

2.2. Cultivation

Precultures were performed with EnPresso B (Enpresso GmbH, Berlin, Germany) medium with 9 U L^{-1} Reagent A at 37 °C in a 24 multi well Oxodish plate to keep the cells in the exponential growth phase (PreSens GmbH, Regensburg Germany). The main culture was started as batch at 37 °C with 5 g L^{-1} glucose. The initial batch phase was prolonged after 1 hour by an additional feed pulse to a final concentration of 5 g L^{-1} glucose. The stirrer speed was kept constant at 3000 rpm. After the end of the batch phase a fed-batch was started with a pulse-based glucose feeding every 5 min with a feed solution with 400 g L^{-1} of glucose dissolved in deionized water. The feeding rate was increased exponentially and switched to a constant feed when the maximum pulse volume of 22 µL was

 doi:10.20944/preprints202009.0381.v1

reached. In total the cultivations were carried out over 8 hours with fed-batch phases of 5.4 to 6.1 hours, depending on the length of the clone-specific batch phases. The μ_{set} for the exponential feed was chosen to be 50 % of the model-predicted μ_{max} value and was adapted in every modelling cycle for each clone. The volume of the feed pulses was determined on the basis of the calculated feed rate. All experiments were carried out as biological triplicates, each triplicate was run on three columns in the same row of the bioreactor system.

2.3. Sampling and Analytic

During the cultivations pH and DOT were measured online in the mini bioreactor system. Each column of the bioreactor system was sampled every 45 min in a sequential mode with a sampling interval of 15 min. Samples were inactivated directly with NaOH in 96 well plates at 4 °C on the deck of the robot until further processing. After 5 samplings the sampling plates were automatically transferred to the Hamilton robot for OD_{600}, glucose and acetate measurements in 96 well plates as described earlier [16]. For the OD_{600} measurements, the samples were diluted to remain in the linear range. The dilution factor was adjusted between 20 and 100 over the course of the cultivation process. All OD_{600} values were multiplied by a correction factor of 2.62 to convert the values to a liquid height of 1 cm. Based on the OD_{600} measurements the dry cell weight of the biomass was calculated by multiplying the OD_{600} with 0.33 [34]. Due to the time-consuming sampling and analysis procedure, the values for biomass, glucose and acetate were written to the database with a delay of 0.25 - 1.35 h for the biomass and 0.66 - 2 h for glucose and acetate, respectively, depending on the column of the bioreactor system where the sample was taken.

In total, during the eight hours of cultivation per reactor 1440 values for DOT and pH, respectively, were collected, as well as 23 samples for biomass (OD_{600}) and each 20 samples for glucose and acetate measurements. For each experiment, the parameter estimation had to consider 1503 measurements leading to a sensitivity matrix of 1503x4x18.

2.4. Strains

The used strains in this study were *E. coli* K-12 W3110 (F^- lambda$^-$ IN(*rrnD-rrnE*)1 rph-1), *E. coli* K-12 BW25113 (F^-, DE(*araD-araB*)567, lacZ4787(del)::*rrnB-3*, LAM$^-$, *rph-1*, DE(*rhaD-rhaB*)568, *hsdR514*) and six knockout strains obtained from the NBRP at the National Institute of Genetics, Shizuoka, Japan (Keio collection [35]), namely *E. coli* BW25113-JW0554-KC (*ΔompT*), *E. coli* BW25113-JW3975-KC (*ΔaceA*), *E. coli* BW25133-JW1907-KC (*ΔfliA*), *E. coli* BW25133-JW2076-KC (*ΔgatC*), *E. coli* BW25113-JW2082-KC (*ΔgatZ*), *E. coli* BW25133-JW2943-KC (*ΔglcB*).

2.5. Computational methods

The *E. coli* macro-kinetic growth model consists of 5 ordinary differential equations describing biomass, glucose, acetate, oxygen, and enzymatic glucose release. The model contains 18 parameters from which 13 have been shown to vary with mutations and cultivation conditions, see [36] for details. Information on the procedure and numerical implementation for the parameter estimation are given in [11]. Cultivation time and data for the different sequential tasks are summarized in Table 1. All measurements used for the parameter estimation are available in the table S1.

Preprints (www.preprints.org) | NOT PEER-REVIEWED | Posted: 17 September 2020 doi:10.20944/preprints202009.0381.v1

Table 1: Underlying data, i.e. number of analysis of sensor data, for the parameter estimates of one biological triplicate.

Sequential task #	Cultivation time [h]	Available measurements			
		DOT	Biomass	Glucose	Acetate
1	1.38	321	6	0	0
2	1.88	411	16	0	0
3	2.55	531	16	10	10
4	3.52	705	26	10	10
5	3.93	780	26	20	20
6	5.17	999	36	20	20
7	5.94	1137	36	30	30
8	6.91	1311	46	30	30
9	7.66	1440	46	40	40

2.6. Parameter estimation

The parameter estimation is formulated as the following optimization problem:

$$\hat{\theta} := \underset{\theta}{\operatorname{argmin}}\ \Phi(U, \theta) \tag{1}$$

Where the objective function formulated as:

$$\Phi(U, \theta) := \sum_{i=1}^{5} \frac{1}{N_i} \sum_{j=1}^{N_i} (y_{i,j}(U, \theta) - y_{i,j}^{m})^2 \tag{2}$$

where $y_{i,j}(U, \theta)$ are the simulated, and $y_{i,j}^{m}$ are the corresponding measured states. The index $i = 1, \dots, 5$ indicates the measured variables and the index $j = 1, \dots, N_i$ indicates individual datapoints. For each state the sum of the squared differences between all measured and simulated datapoints is normalized by the number of datapoints.

All computations, i.e. the numerical solution of the dynamical model, the estimation of kinetic growth parameters, and the computation of optimal cultivation conditions are written in MATLAB (The MathWorks, Inc., Natick, Massachusetts, USA). The parameter estimation is solved with the interior-point algorithm using the wrapper from MATLAB. The states of the model and their sensitivities are computed using CVODE available in the SUNDIALS Toolbox [37]. Initial values, lower and upper bounds of the parameter estimation are based on expert's knowledge and summarized in table S2. The PE is regularized using the Subset Selection method described by Lopez et al. embedded in the optimization. The algorithm implements a stepwise forward selection of parameters to be included in the estimation problem based on the dynamical parameter sensitivities. Identifiable parameters are selected by a ranking of all parameters according to linear independence and an analysis of the matrix rank condition of the sensitivity matrix.

2.7. Feed calculation

The exponential feed was calculated using the standard fed-batch equation [39] which was adapted to consider a pulse based profile. It is computed as:

$$F_t = F_0\, e^{\mu_{set} t} \tag{3}$$

where F_t ($L\ h^{-1}$) represents the feed rate at time point t and μ_{set} (h^{-1}) the targeted specific growth rate. F_0 is the initial feed rate and $t = 0$ the time of the feed start. Since the feed in a fed-batch process is the only major volume changing factor, volume changes due to sampling is neglected at this point, the volume change could be described as

Preprints (www.preprints.org) | NOT PEER-REVIEWED | Posted: 17 September 2020 doi:10.20944/preprints202009.0381.v1

$$\int_{V_0}^{V} dV = F_0 \int_{t_0=0}^{t} e^{\mu_{set} \cdot t} dt = \frac{F_0}{\mu_{set}} e^{\mu_{set} \cdot t}|_0^t \quad (4)$$

The pulse volume is calculated as

$$V = V_0 + \frac{F_0}{\mu_{set}} (e^{\mu_{set} \cdot t} - 1) \quad (5)$$

with

$$F_0 = \frac{\mu_{set}}{Y_{X/S} * S_i} X_0 V_0 \quad (6)$$

Where $Y_{X/S}$ $[g\ g_x^{-1}]$ is the Yield coefficient of glucose per biomass, S_i $[g\ L^{-1}]$ the glucose concentration in the feed solution, X_0 $[g]$ the biomass concentration and V_0 the volume at the feed start. Volume manipulations by the pipetting robot (e.g. volume balancing, sampling, base addition for pH control) are considered in the feed calculation apart of the equations above.

Biomass and volume for the calculation of F_0 (eq. 6) were estimated by simulations based on the current parameter set. The end of the batch phase was defined as the time point where the predicted glucose and acetate concentrations were below 0.02 g L^{-1}. If the acetate consumption was slow, the feed was started anyway no later than 45 min after the depletion of glucose.

3. Results

Eight different *E. coli* K-12 clones were cultivated in parallel with an industrial process-relevant feeding design consisting of batch, exponential fed-batch and constant feed phases. The feed is applied as pulses to expose the cells to inhomogeneities similar to those in large-scale bioreactors.

3.1. Parallel cultivation

The length of the batch phase varied between the and lasted 1.65 h for *E. coli* W3110 (the fastest growing clone) and 1.86 h for *E. coli* BW25113 *ΔglcB* (the slowest growing clone). After the end of the batch phase the feed was automatically started. Due to the pulse nature of the feed procedure the feed start is visible through the oscillating DOT values (see **Error! Reference source not found.**a). These oscillations, as well as the glucose at-line data proof that glucose limitation was maintained during the fed-batch phase in all cultivations. Furthermore, no significant acetate accumulation was observed (**Error! Reference source not found.**b). The cultivations show a low variance between triplicates which is obvious from the online DOT and pH profiles as well as from the automatically analysed glucose and acetate values. Nine glucose data points were detected as possible outliers (at 6.14 and 7.14 hours). However, no technical issues were found to explain the sudden drift. In the case of *E. coli* W3110, the biomass of one triplicate was also lower, due to oxygen limitation. This could mean that the higher glucose concentration would indicate overfeeding. As expected, the pH decreased during the batch phase and started to increase after glucose depletion (typically caused by acetate consumption). During each glucose pulse cycle, perturbation of pH is observed which is caused by the transient production of acetic acid (**Error! Reference source not found.**c). Finally, a small increase in the pH was observed after the switch to constant pulse based feed.

3.2. Prediction of batch and feed start

The first model calibration cycle (cf. Figure 1) was initiated after 1.4 hours of batch cultivation. During the batch phase the feed start time and initial biomass were re-computed using the updated model parameters after the first measurement. The end of batch was defined as the time point at which glucose as well as the acetate (produced during overflow growth) were depleted. Therefore, the fed-batch phase in our cultivations started purposely later compared to typical fed-batch processes which are mostly started when glucose is depleted, and the DO signal increases. Note that

 doi:10.20944/preprints202009.0381.v1

feeding was started only when acetate had been metabolised. This prevents possible overfeeding with glucose by co-metabolism of the remaining acetate and thus allowed a higher process stability.

Preprints (www.preprints.org) | NOT PEER-REVIEWED | Posted: 17 September 2020 doi:10.20944/preprints202009.0381.v1

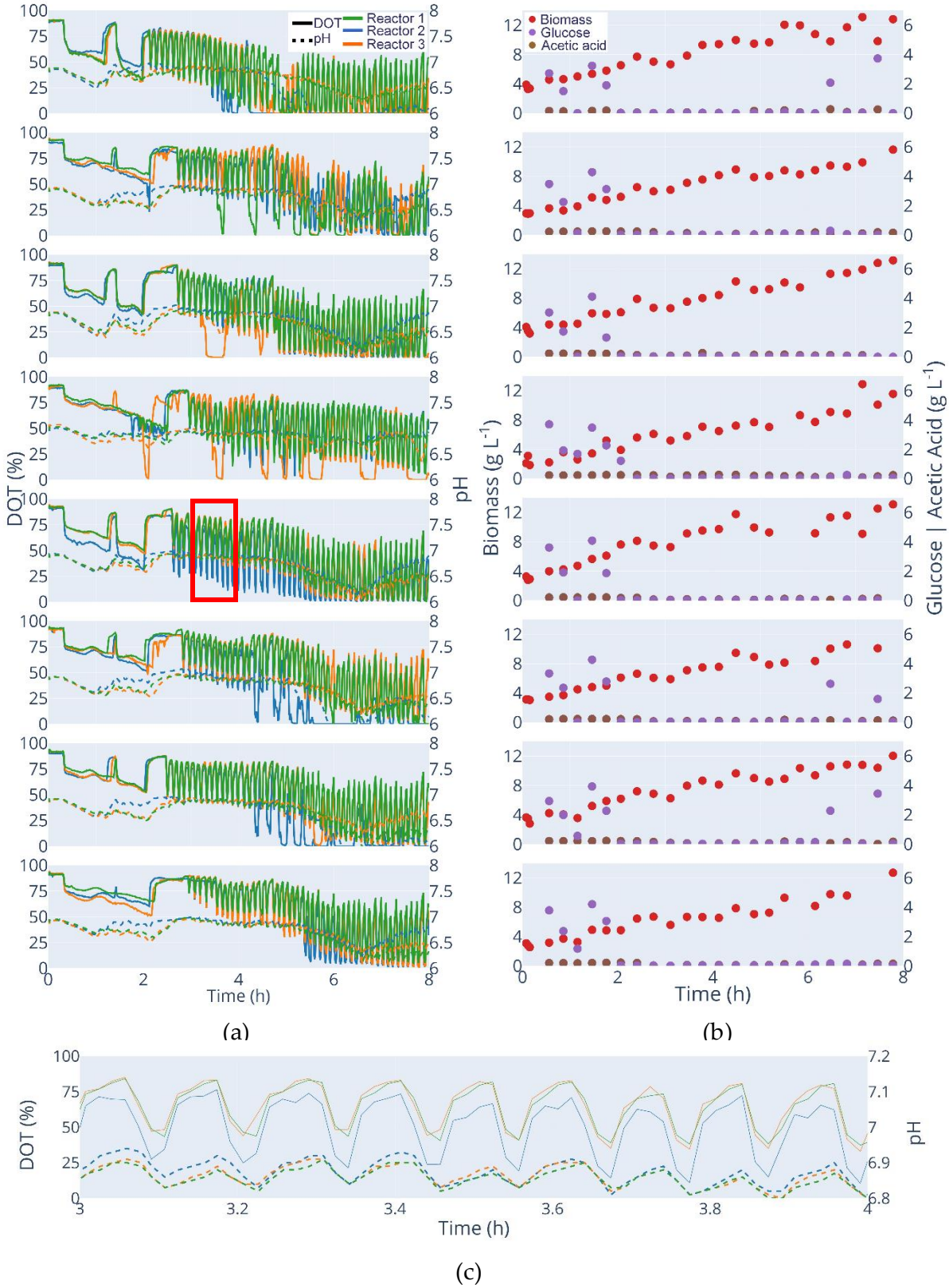

Figure 2: Cultivation data of all used strains; Clones from top to bottom: *E. coli* W3110; *E. coli* BW25113; *E. coli* BW25113 *ΔompT*; *E. coli* BW25113 *ΔaceA*; *E. coli* BW25113 *ΔfliA*; *E. coli* BW25113 *ΔgatC*; *E. coli* BW25113 *ΔgatZ*; *E. coli* BW25113 *ΔglcB* (a) DOT [%]: solid lines, pH: dotted lines; (b) Biomass [g L^{-1}]: red dots; Glucose [g L^{-1}]: purple dots; acetic acid [g L^{-1}]: brown dot. (c): illustration of the oscillating pH values with each glucose pulse. The figure shows the section marked in (a) red. An interactive version of (a) and (b) is available at http://www.bioprocess.tu-berlin.de/fileadmin/fg187/Publications/Hans_2020/fig2.html

Preprints (www.preprints.org) | NOT PEER-REVIEWED | Posted: 17 September 2020 doi:10.20944/preprints202009.0381.v1

Figure 3a illustrates the outcome of the model calibration cycle during the batch phase, at the example of the *E. coli* BW25113 *ΔglcB* cultivations data (grey cross) and simulations after model calibration (blue line). It is obvious that the first parameter estimate indicates for this strain a slower growth compared to the initial parameter set. However, with every model calibration cycle, the computed growth rate (μ_{max}) increased from 0.36 h^{-1} at t_1 to 0.58 h^{-1} at t_2 and up to 0.82 h^{-1} at the third shown model calibration cycle. The fit to the cultivation data is improved with each modelling cycle and the trend of the cultivation is well represented, at least after the third modelling cycle.

In addition, due to the underestimated μ_{max}, the first model calibration cycle failed to propose the end of the batch phase properly. An accurate estimation of the specific glucose consumption rate is only reached after the glucose had been used up, but then the estimation is very precise. Although, the end of the batch phase is equally estimated in the third model calibration cycle and in the initial unadjusted model (black dashed lines, Figure 3a; 1.94 h and 1.92 h), the feed (Figure 3b) started 21 min later (2.40 h and 2.01 h). This is because of differences in the production and consumption rate of acetate resulting in different starting times of the fed-batch phase. Based on the DOT profiles, acetate was consumed after 2.5 hours; this also corresponds well with the at-line measurements of (Figure 2, supplementary table S1).

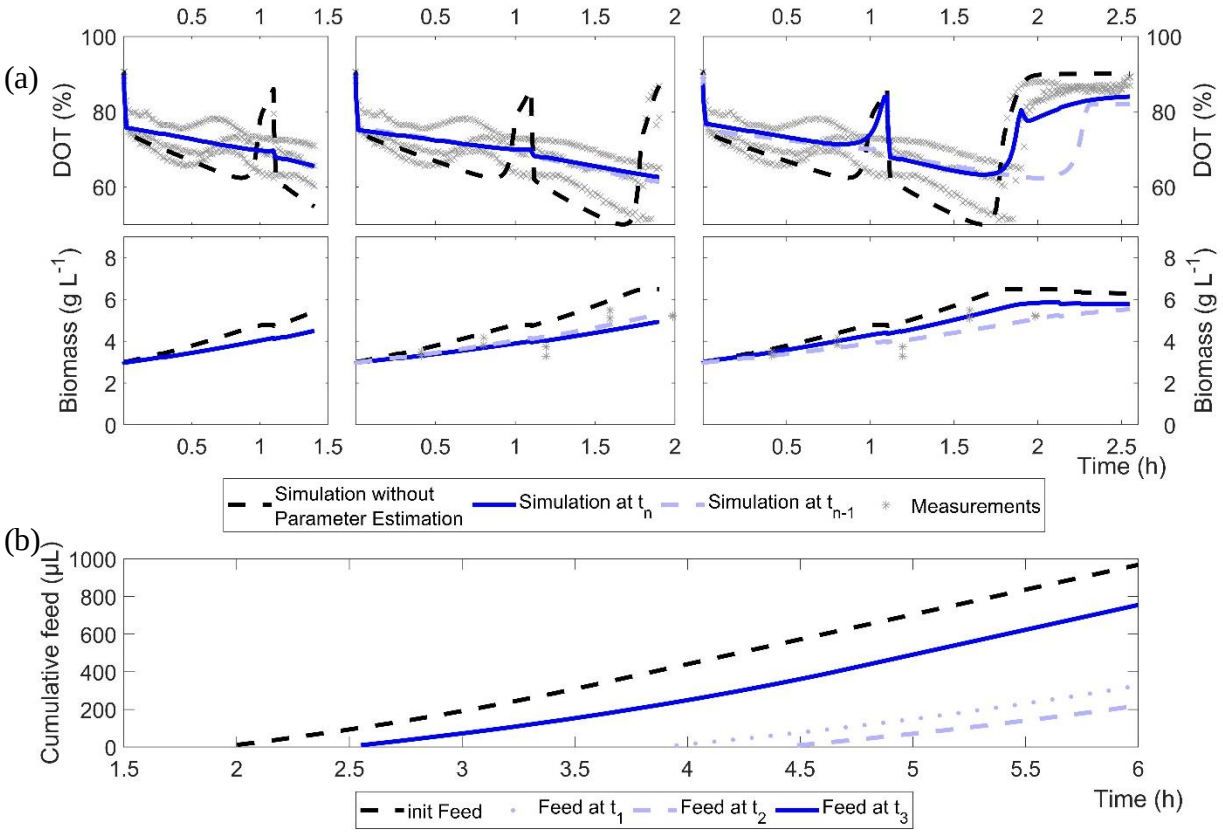

Figure 3: Illustration of the results of the sequential tasks 1 to 3 for the cultures of *E. coli* BW25113 *ΔglcB*. (a): Comparison of parameter estimation results at different times during the cultivation, the initial parameter set and the measurements for strain *E. coli* BW25113 *ΔglcB*; (b): Results for computed feeding profiles after the sequential task 1-3 as cumulative volume.

The predicted end of the batch phase is very close to the observed one in all cultivations even after the second model calibration and 1.5 hours of cultivation (Table 2). Due to minor variations in the initial biomass concentrations the calculated batch end differs from clone to clone, already with the initial model and with an equal parameter set. For some cultivations the time of glucose depletion was predicted with an accuracy of less than one minute (*E. coli* BW25113 *ΔgatZ*). In the worst case the time of glucose depletion was predicted 22.8 min too late (*E. coli* BW25113 *ΔaceA*). A missed batch

Preprints (www.preprints.org) | NOT PEER-REVIEWED | Posted: 17 September 2020 doi:10.20944/preprints202009.0381.v1

end and even a short starvation phase could lead in unwanted metabolic reactions by the strain and can influence the process and product quality. However, in this cultivation triplicate, one cultivation can be considered as outlier (Figure 2a) and a difference of 22 min is still in an operational range. Due to operational reasons the model calibration with all clones was maintained. The mean difference between the observed and predicted time points for glucose depletion is 6.9 min for the calibrated model after 1.5 hours and thus better compared to the initial model with a mean prediction error of 7.3 min.

Complete consumption of acetate is only observed for five of the eight strains. For all these strains the adjusted model predicts the acetic acid consumption better compared to the initial model, with the exception of *E. coli* BW25113 *Δomp*. Complete consumption of acetic acid was not observed for three clones, because of the time depending restrictions in the feed (maximum tolerance between end of glucose depletion and feed start, see section 0). However, for these three clones the initial model predicted a faster and the adjusted model a slower acetic acid consumption rate. The times of the first feed pulse are summarized in Table 2 (Feed start), the predicted end of batch and the first pulse may differ due to technical reasons (delay in computation or first pulses are calculated with 0 µL due as the minimal pipetting volume restrictions).

Table 2: Batch end prediction overview: initial, adjusted (parameter estimation after 1:52 hour) and observed times for consumption of glucose and acetate and the actual feed start based on the first executed glucose pulse.

Strain	Glucose consumption [hh:mm]			Acetate consumption [hh:mm]			Feed start [hh:mm]
	initial	adjusted	Observed	initial	adjusted	observed	
E. coli W3110	01:46	01:40	01:39 ± 00:01	02:03	01:48	01:48	01:55
E. coli BW25113	01:52	01:38	01:49 ± 00:03	02:00	03:02	> 02:23	02:23
E. coli BW25113 *ΔompT*	01:46	01:40	01:40 ± 00:01	01:53	03:05	02:10	02:23
E. coli BW25113 *ΔaceA*	02:13	02:11	01:48 ± 00:21	02:22	03:06	> 02:37	02:37
E. coli BW25113 *ΔfliA*	01:51	01:36	01:42 ± 00:01	01:59	02:13	02:07	02:16
E. coli BW25113 *ΔgatC*	01:49	01:39	01:46 ± 00:05	01:57	02:50	02:25	02:30
E. coli BW25113 *ΔgatZ*	01:46	01:43	01:43 ± 00:01	01:55	03:03	> 02:09	02:09
E. coli BW25113 *ΔglcB*	01:55	01:56	01:51 ± 00:03	02:03	02:24	02:30	02:37

3.3. Feed and fed-batch

During the fed-batch phase the size of the feed pulses is re-computed during each model calibration cycle. Based on the new parameter set the maximal glucose uptake rate was determined as basis for the new feeds. With the exception of *E. coli* BW25113 *ΔglcB* (**Error! Reference source not found.** (h)), the first feed rate (grey bars) was higher than the following calculated feed pulses. However, the second applied feed rates for *E. coli* BW25113 *ΔompT*, *E. coli* BW25113 *ΔfliA* and *E. coli* BW25113 *ΔgatZ* (**Error! Reference source not found.** (c), (d) and (f)) were close to the initial feed rates but were reduced in the later model calibration cycles. In the case of *E. coli* BW25113 *ΔglcB* the second feed is somewhat higher than the later one, which is reflected in both the initial feed rate and in the slope of the feed (all feed pulses are summarised in **Error! Reference source not found.**). Feed pulses are calculated by the optimisation algorithm for each strain and applied to all biological triplicates. In this way, eight different feeding rates were calculated, and 24 cultivations were carried out in parallel.

Preprints (www.preprints.org) | NOT PEER-REVIEWED | Posted: 17 September 2020 doi:10.20944/preprints202009.0381.v1

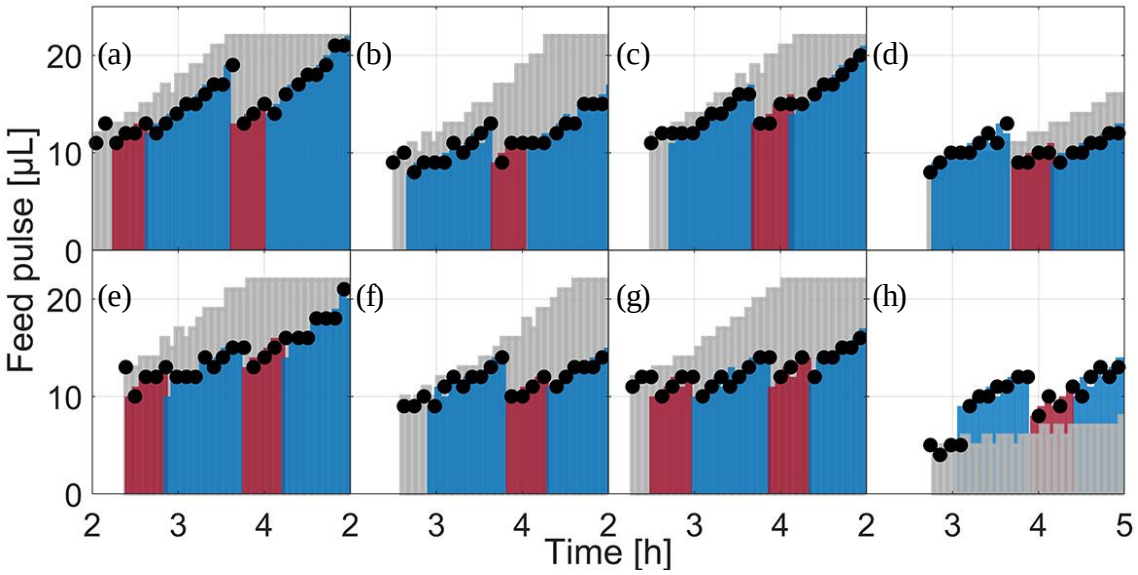

Figure 4: The applied feed and scheduled feeds for each strain between cultivation hour 2 and 5. **Black dots**: the applied feed based on the real executed feed, logged by the LHS; **Light grey bars**: scheduled feed at feed start; **coloured bars**: scheduled feeds in the following modelling cycles, the colour change indicates the next modelling cycle. (a) *E. coli* W3110; (b) *E. coli* BW25113; (c) *E. coli* BW25113 *ΔompT*; (d) *E. coli* BW25113 *ΔaceA*; (e) *E. coli* BW25113 *ΔfliA*; (f) *E. coli* BW25113 *ΔgatC*; (g) *E. coli* BW25113 *ΔgatZ*; (h) *E. coli* BW25113 *ΔglcB*

3.4. Parameter estimation

During all model calibration cycles the model parameters are estimated on the basis of all available data, i.e. all data which were collected from the start of the cultivations to the actual time point. For all strains, the measurements and dynamics of cultivation are well represented in the simulation of the calibrated model as illustrated in Figure 5 for the strain *E. coli* BW25113 *ΔglcB* (last modelling cycle, for the other strains see supplementary figures S1-7). In contrast to the calibrated model, the initial model overestimated the biomass formation. This trend could be observed for all strains. The DOT measurements indicate a slower glucose uptake than predicted. A lower specific glucose uptake rate was calculated in the first two modelling calibration cycles compared to the later ones (see Figure 3). The lack of the glucose measurement results in the first two model calibration cycles is caused by the time delay in the at-line analytics. The prediction accuracy of acetic acid is increased in the batch and fed-batch phase after model calibration. The cultivation dynamics are well fitted. The parameters to be adjusted in each model calibration cycle are selected by the included subset selection. The parameters K_{ap}, k_La and q_m, are not adjusted in one model calibration cycle; K_o, K_{sq}, Y_{ofm} and Y_{oresp} are only partly selected for parameter estimation (Figure 6, all parameter sub-sets are shown the Supplementary Table S2). Regularization of parameter estimation using a subsets selection method [38] was used to ensure a meaningful parameter set. Monte Carlo simulations have shown to give a good insight into the actual, non-linear parameter distribution [40] and were therefore performed to get a better understanding of the parameter correlation.

Preprints (www.preprints.org) | NOT PEER-REVIEWED | Posted: 17 September 2020 doi:10.20944/preprints202009.0381.v1

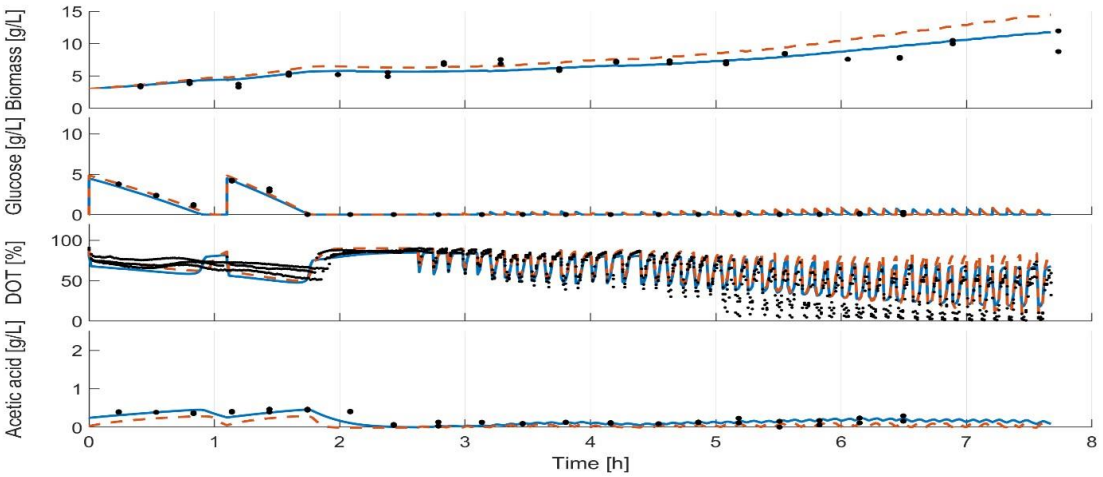

Figure 5: Model for *E. coli* BW25113 $\Delta glcB$ after the last model calibration cycle and at the beginning of the experiment. Solid line: calibrated model; dashed line: initial model; dots: measurements.

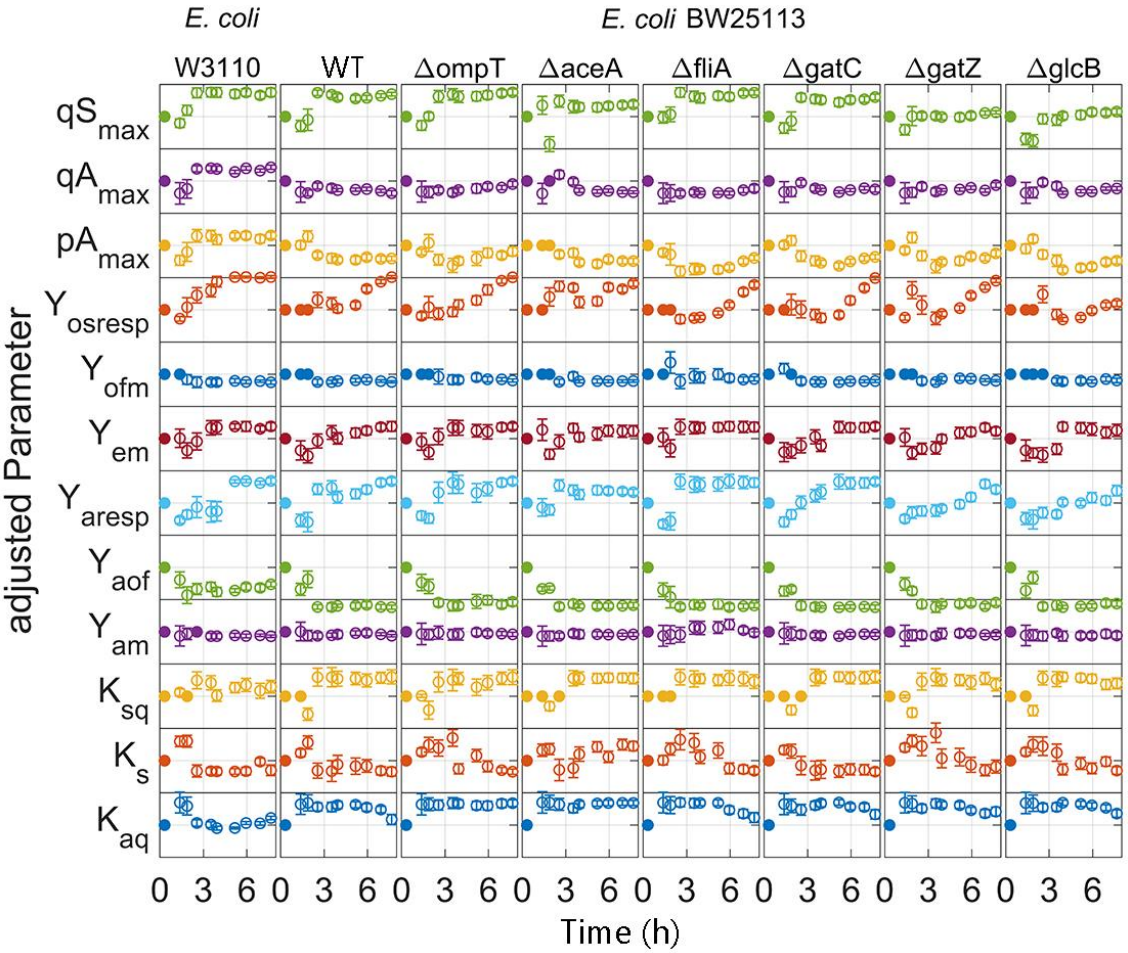

Figure 6: Adjusted parameters of the time for each *E. coli* strain: Parameters are normalized to the initial value and scaled to 3 times of the standard derivation. **Filled dots**: parameter is fixed by the sub set selection; **open dots**: estimated parameter

Preprints (www.preprints.org) | NOT PEER-REVIEWED | Posted: 17 September 2020 doi:10.20944/preprints202009.0381.v1

The correlation between all parameters is very weak. Only, K_{aq} and K_{sq} showed a correlation with qA_{max}. K_{aq} and K_{sq} are the affinity constants for acetate and glucose uptake, respectively, and a dependence to the maximal acetate uptake rate (qA_{max}) cannot be avoided in the model. Parameter distribution as well as pairwise correlation of the adapted parameters for *E. coli* BW25113 *ΔglcB* (last model calibration cycle) is summarized in Figure 7. The high significance of each parameter is indicated by the narrow distribution and low variation for the most important model parameters (Table 3), especially for **Error! Bookmark not defined.** the parameters for Y_{em}, qS_{max} and $Y_{osresp.}$ Normal distribution is given for all parameters except for Y_{am}. This parameter is quite close to the lower bound of the previously defined solution space. It is noted that this situation should be avoided as it might reduce the accuracy of the parameter estimates. The parameter distribution of all other strains at the last modelling cycle are disposed in the supplementary Figures S09-S16.

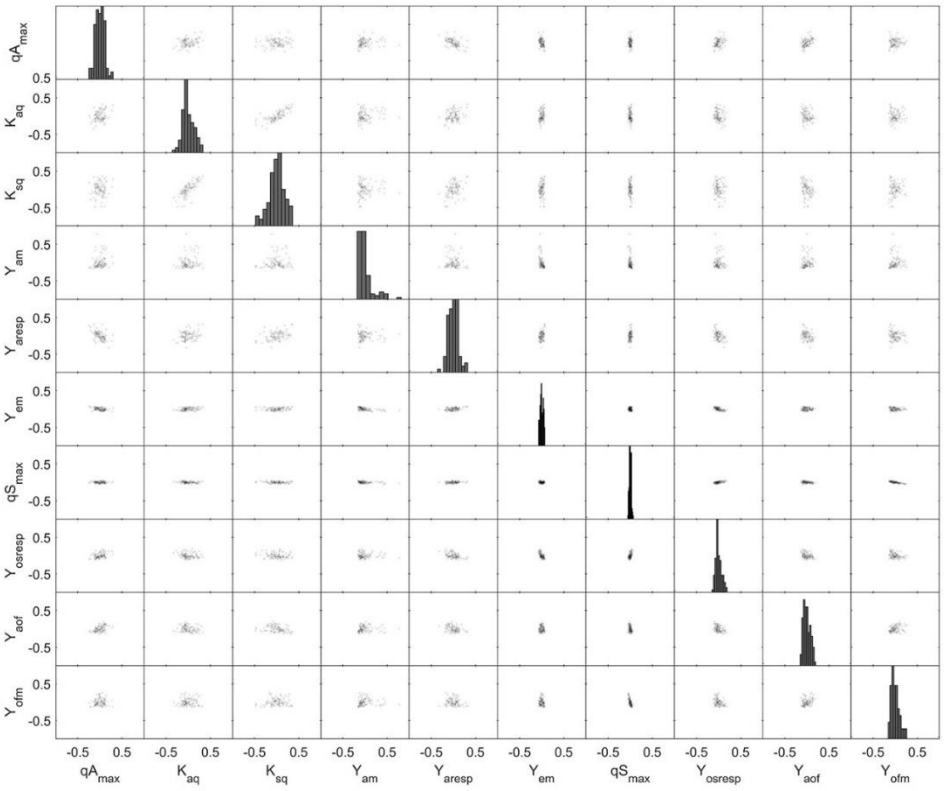

Figure 7 Monte Carlo parameter estimation: Pair plots of the 500 best Monte Carlo parameter estimation results with the regularized parameter set based on the dataset for *E. coli* BW25113 *ΔglcB* during the last modelling cycle. Monte Carlo simulations were carried out with $\sigma = 0.15$ for biomass, glucose, acetate and $\sigma = 0.05$ for DOT.

Table 3: Values, variance and relative variance of the adjusted parameters for all clones after the final model calibration cycle.

Parameter	Unit	inital guess	*E.coli* W3110			*E. coli* BW215113																				
						WT			ΔompT			ΔaceA			ΔfliA			ΔgatC			ΔgatZ			ΔglcB		
			θ	σ_θ	$\%\sigma_\theta$	θ	σ_θ	$\%\sigma_\theta$	θ	σ_θ	$\%\sigma_\theta$	θ	σ_θ	$\%\sigma_\theta$	θ	σ_θ	$\%\sigma_\theta$	θ	σ_θ	$\%\sigma_\theta$	θ	σ_θ	$\%\sigma_\theta$	θ	σ_θ	$\%\sigma_\theta$
qAmax	$g\,g^{-1}\,h^{-1}$	1,0252	1,59	0,11	6,78	0,52	0,11	21,74	0,90	0,05	5,92	0,56	0,15	26,05	0,72	0,11	15,59	0,68	0,08	12,19	0,86	0,10	11,54	0,71	0,07	9,54
Kaq	$g\,L^{-1}$	0,2133	0,59	0,14	23,11	0,55	0,09	16,28	0,98	0,07	7,11	0,98	0,14	13,82	0,60	0,12	20,70	0,68	0,10	14,16	0,75	0,12	15,97	0,70	0,04	6,24
Ksq	$g\,L^{-1}$	1,0667	1,52	0,33	21,71	1,98	0,34	16,98	1,97	0,26	13,17	1,91	0,32	16,95	1,77	0,29	16,26	1,99	0,25	12,35	1,63	0,31	18,80	1,68	0,34	20,14
Yam	$g\,g^{-1}$	0,1955	0,40	0,03	7,18	0,41	0,04	10,79	0,44	0,05	10,16	0,44	0,08	18,79	0,48	0,04	8,04	0,44	0,08	17,80	0,44	0,04	8,89	0,42	0,03	6,82
Yaresp	$g\,g^{-1}$	0,1672	0,15	0,01	4,94	0,15	0,01	5,09	0,15	0,01	4,55	0,12	0,01	8,36	0,15	0,01	4,79	0,15	0,01	8,02	0,13	0,01	6,65	0,13	0,00	3,44
Yem	$g\,g^{-1}$	0,56	0,60	0,01	2,48	0,60	0,01	1,82	0,60	0,02	2,89	0,58	0,02	2,70	0,60	0,01	1,94	0,60	0,02	3,27	0,58	0,01	2,19	0,59	0,01	1,53
qSmax	$g\,g^{-1}\,h^{-1}$	1,3431	1,60	0,02	1,20	1,58	0,03	2,09	1,60	0,03	2,02	1,47	0,03	1,79	1,59	0,03	1,83	1,55	0,03	2,08	1,39	0,02	1,16	1,40	0,04	2,54
Ks	$g\,L^{-1}$	0,05	0,03	0,01	22,73	0,03	0,00	15,72	0,03	0,01	27,93	0,08	0,01	8,44	0,03	0,01	19,59	0,03	0,01	21,88	0,04	0,01	29,35	0,03	0,01	18,79
Ko	$g\,L^{-1}$	1	19,87	1,52	7,64	18,13	1,87	10,32	14,51	1,27	8,76	18,64	1,93	10,38	16,29	1,66	10,17	16,00	2,22	13,88	14,13	0,95	6,69	9,57	1,27	13,28
Yosresp	$g\,g^{-1}$	1	2,00	0,05	2,54	2,00	0,04	1,90	1,99	0,09	4,46	1,80	0,09	4,78	1,76	0,05	3,03	1,97	0,08	4,31	1,89	0,06	3,04	1,19	0,02	2,03
pAmax	$g\,g^{-1}\,h^{-1}$	1,3091	1,60	0,07	4,18	0,93	0,12	13,29	1,13	0,08	7,31	0,86	0,07	8,64	0,95	0,07	7,45	0,98	0,09	8,96	1,08	0,09	8,37	0,87	0,09	10,77
Yaof	$g\,g^{-1}$	0,4607	0,35	0,01	3,88	0,20	0,02	12,23	0,24	0,02	7,52	0,21	0,02	6,99	0,21	0,02	7,05	0,20	0,02	8,88	0,23	0,02	8,21	0,23	0,02	7,91
Yofm	$g\,g^{-1}$	0,2795	0,20	0,01	4,74	0,20	0,02	7,53	0,22	0,01	5,46	0,21	0,02	9,87	0,23	0,01	5,75	0,21	0,02	10,21	0,22	0,01	5,20	0,22	0,01	5,08

Preprints (www.preprints.org) | NOT PEER-REVIEWED | Posted: 17 September 2020 doi:10.20944/preprints202009.0381.v1

In the present work, eight strains were examined in 24 successful cultivations. The end of glucose uptake was in part predicted with small errors of less than one minute, thanks to the iterative model calibration cycle. The feed start was automatic and in an operable acceptable time window using the dynamic process redesign as defined in the model calibration cycle. The parameter sets estimated are always unique and with a physiological meaning even with very little data in the initial phase of this study, e.g. the first 3 hours. This is ensured by the built-in subset selection and is proofed by the Monte Carlo simulations made afterwards.

4. Discussion

In this study we presented a computational framework able to design and operate parallel *E. coli* cultivations without human supervision. The results demonstrate that a robust operation tailored to each specific clone is possible through an adaptive input design. Undesired experimental conditions (e.g. overfeeding and starvation) are avoided while sufficient information to allow for a confident discrimination of the strains is generated. Both, start time and feed rate were accurately predicted for each one of the eight strains, using feedback information from the online and at-line measurements during the cultivation. This is essential in an experimental facility aimed to perform screening cultivations for clones whose phenotype is not known beforehand. The relevance of an adaptive and specific experimental design can be seen in this case study. As illustrated in **Error! Reference source not found.**, despite the fact the strains characteristics differ only minimally from each other, an experiment with a fixed start time and feeding rate would have violated important experimental constrains.

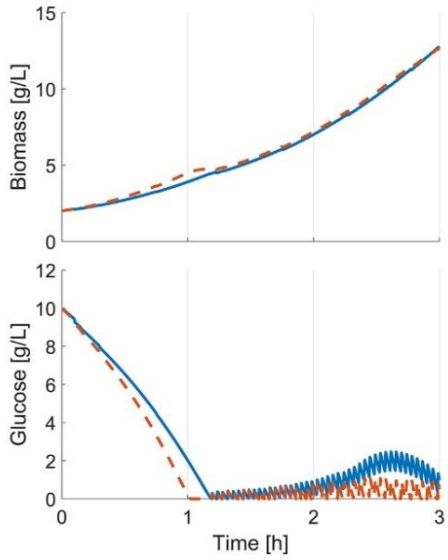

Figure 8 In-silico comparison of different hosts: Simulation based on last modelling cycle parameter set. Initial values: Glucose 10 g*L^{-1}, Biomass 2 g/L. Solid line: *E. coli* BW25113 dashed line: *E. coli* BW25113 Δ*gatZ*. Feed start is simulated at 2.3 hours, μ_{set} is fixed at 0.5 h^{-1}. If the feed start and rate is only adjusted to one strain, the cultivation of the Δ*gatZ* mutant would lead to overfeeding.

Additionally, the use of a macro-kinetic growth model that describes the main extracellular dynamics of *E. coli* was shown to be sufficient. In average the predicted feed start differs by less than 10 min for the optimal one, which is in an acceptable range and is mainly caused by unobserved disturbances in the system. If necessary, the mismatch can be further reduced by increasing the frequency of model adaptations.

As expected, the parameter variance in general decreases with every model calibration cycle. However, some parameters could not or only with insufficient confidence be identified. This hampered a distinction of some essential parameters as like the maximal acetate uptake rate (qA_{max}). Despite this, the quantification of the reliability of the outputs as presented by Anane et al [41] allows the differentiation of the main parameter, e.g. the maximal glucose uptake (qS_{max}) with statistical significance (see **Error! Reference source not found.**).

Nevertheless, statements on the performance of the clones can be made using the model parameters. The final results show that Δ*ompT* has the largest qS_{max} value and Δ*gatZ* the lowest. Furthermore, the parameter identifiability can be increased in future applications using methods for Optimal Experimental Design (OED) [24,42].

The macro-kinetic model used in this study is clearly insufficient to describe the complex nonlinear dynamics of the system. Still, we overcome this issue by the adaptive nature of the framework since a proper prediction within the current horizon is sufficient to assure a robust operation of the cultivations. The variations on the parameters caused by intracellular changes in the metabolic machinery together with heterogeneous mutations in the population [43] are shown in

 doi:10.20944/preprints202009.0381.v1

(Figure 6). Therefore, an iterative recalculation of the feed is necessary to cope with disturbances in the experiments and inaccuracies in the model.

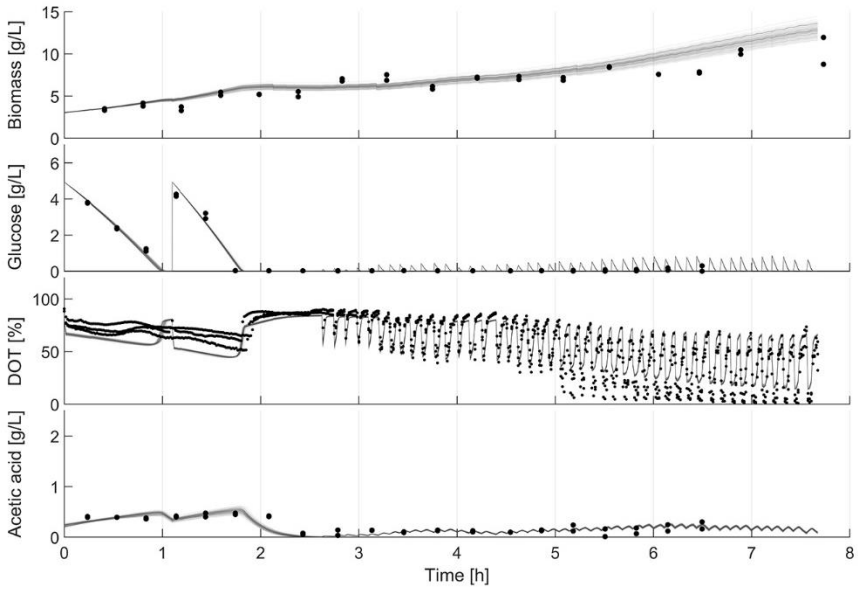

Figure 9 Model uncertainty based on parameter standard deviation: Monte Carlo simulation: Results of 1000 parameter estimates based on in-silico data. In silico data were generated based on the last data set for *E. coli* BW25113 $\Delta glcB$ and by random σ of 0.15 for biomass, glucose, acetate, and a σ of 0.05 for DOT.

The frequency of the parameter estimation was defined based on the availability of at-line data (biomass, glucose and acetate) and as expected, the at-line data are decisive to achieve model identifiability. Still, the results show that especially parameters related to glucose consumption can be identified using only the online DOT signal. This shows that, even though in a significantly limited manner, the framework can also be used to increase the robustness of robotic facilities that do not have embedded at-line analytics. The glucose consumption rate seems to be observable from the DOT signal by which a reduced version of the macro-kinetic model could be used to build an observer based feeding control [44]. Finally, we also demonstrated that the length of the batch phase is essential to assure sufficient data before the start of the feeding so as to allow a reliable operation of the following phases.

5. Conclusions

The operation of robotic experiments with multiple fed-batch cultivations in parallel is very challenging even for skilled operators, since many decisions and tasks are needed at the same time. In this work we present an adaptive framework for conditional screening for parallel fed-batch experiments aiming to identify the best candidate strain for industrial scale biomanufacturing. We demonstrate that the use of a macro-kinetic growth model in an adaptive framework using online and at-line data information in a feedback loop is necessary to:

1. design a specific strategy for each different strain of the screening experiment
2. increase the robustness of the robotic operation against experimental disturbance, and
3. give an approximation of the reliability of the simulation results with respect to production scale performance.

To our knowledge, this is the first successful model-based operation of 24 fed-batch cultivations with as much as eight different strains in parallel including its characterization. The results clearly demonstrate the capabilities of the framework to increase the efficiency of combined mini-bioreactor systems with liquid handling stations to drastically reduce the experimental time, efforts, and failure rate in High Throughput Bioprocess Development.

 doi:10.20944/preprints202009.0381.v1

Supplementary Materials Tables S1 all experimental measurements used for the modelling cycles; Table S2: all parameter sets; Figure S1-7

Author Contributions: Conceptualization, MNCB. and SH.; methodology, SH.; software, SH and BH; validation, SH and MNCB.; formal analysis, SH; investigation, SH and MNCB; resources, SH, NK, BH and MNCB; data curation, SH, BH, NK.; writing—original draft preparation, SH.; writing—review and editing, MNCB, TB, PN, NK.; visualization, SH.; supervision, MNCB and PN.; project administration, SH and MNCB; funding acquisition, PN.

Funding: The authors acknowledge financial support by the German Federal Ministry of Education and Research (BMBF) within the European program EraSysApp (grant number: 031L0018A, Leanprot project), which is managed by the Project Management Agency Jülich (PTJ).

Acknowledgments: We would like to thank Robert Giessmann and Terrance Wilms for their programming and modelling support. We acknowledge support by the Open Access Publication Fund of TU Berlin.

Conflicts of Interest: The authors declare no conflict of interest.

References

[1] M. Funke, S. Diederichs, F. Kensy, C. Müller, J. Büchs, The Baffled Microtiter Plate : Increased Oxygen Transfer and Improved Online Monitoring in Small Scale Fermentations, Biotechnol. Bioeng. 103 (2009) 1118–1128. doi:10.1002/bit.22341.

[2] W.A. Duetz, Microtiter plates as mini-bioreactors: miniaturization of fermentation methods, Trends Microbiol. 15 (2007) 469–475. doi:10.1016/j.tim.2007.09.004.

[3] D. Quaglia, M.C.C.J.C. Ebert, P.F. Mugford, J.N. Pelletier, Enzyme engineering: A synthetic biology approach for more effective library generation and automated high-throughput screening, PLoS One. 12 (2017) 1–14. doi:10.1371/journal.pone.0171741.

[4] N.H. Janzen, G. Striedner, J. Jarmer, M. Voigtmann, S. Abad, D. Reinisch, Implementation of a Fully Automated Microbial Cultivation Platform for Strain and Process Screening, Biotechnol. J. 14 (2019) 1800625. doi:10.1002/biot.201800625.

[5] P. Neubauer, M.N. Cruz-Bournazou, F. Glauche, S. Junne, A. Knepper, M. Raven, Consistent development of bioprocesses from microliter cultures to the industrial scale, Eng. Life Sci. 13 (2013) 224–238. doi:10.1002/elsc.201200021.

[6] H. Morschett, L. Freier, J. Rohde, W. Wiechert, E. Von Lieres, M. Oldiges, A framework for accelerated phototrophic bioprocess development: Integration of parallelized microscale cultivation, laboratory automation and Kriging-assisted experimental design, Biotechnol. Biofuels. 10 (2017) 1–13. doi:10.1186/s13068-017-0711-6.

[7] F. Glauche, J. Glazyrina, M.N. Cruz Bournazou, G. Kiesewetter, F. Cuda, D. Goelling, A. Raab, C. Lang, P. Neubauer, Detection of growth rate-dependent product formation in miniaturized parallel fed-batch cultivations, Eng. Life Sci. 17 (2017) 1215–1220. doi:10.1002/elsc.201600029.

[8] D. Weuster-Botz, Experimental design for fermentation media development: Statistical design or global random search?, J. Biosci. Bioeng. 90 (2000) 473–483. doi:10.1016/S1389-1723(01)80027-X.

[9] J. Newton, R. Oeggl, N.H. Janzen, S. Abad, D. Reinisch, Process adapted calibration improves fluorometric pH sensor precision in sophisticated fermentation processes, Eng. Life Sci. 20 (2020) 331–337. doi:10.1002/elsc.201900156.

[10] F. Delvigne, P. Goffin, Microbial heterogeneity affects bioprocess robustness: Dynamic single-cell analysis contributes to understanding of microbial populations, Biotechnol. J. 9 (2014) 61–72. doi:10.1002/biot.201300119.

[11] E. Anane, Á.C. García, B. Haby, S. Hans, N. Krausch, M. Krewinkel, P. Hauptmann, P. Neubauer, M.N. Cruz Bournazou, A model-based framework for parallel scale-down fed-batch cultivations in mini-bioreactors for accelerated phenotyping, Biotechnol. Bioeng. (2019). doi:10.1002/bit.27116.

[12] A. Knepper, M. Heiser, F. Glauche, P. Neubauer, Robotic Platform for Parallelized Cultivation and Monitoring of Microbial Growth Parameters in Microwell Plates, J. Lab. Autom. 19 (2014) 593–601. doi:10.1177/2211068214547231.

[13] P. Neubauer, F. Glauche, M.N. Cruz-Bournazou, Editorial: Bioprocess Development in the era of digitalization, Eng. Life Sci. 17 (2017) 1140–1141. doi:10.1002/elsc.201770113.

[14] S.A. Nicolaou, S.M. Gaida, E.T. Papoutsakis, A comparative view of metabolite and substrate stress and tolerance in microbial bioprocessing: From biofuels and chemicals, to biocatalysis and bioremediation, Metab. Eng. 12 (2010) 307–331. doi:https://doi.org/10.1016/j.ymben.2010.03.004.

[15] J. Hemmerich, S. Noack, W. Wiechert, M. Oldiges, Microbioreactor Systems for Accelerated Bioprocess Development, Biotechnol. Journa. 13 (2018) 1–25. doi:10.1002/biot.201700141.

[16] B. Haby, S. Hans, E. Anane, A. Sawatzki, N. Krausch, P. Neubauer, M.N. Cruz Bournazou, Integrated Robotic Mini Bioreactor Platform for Automated, Parallel Microbial Cultivation With Online Data Handling and Process Control, SLAS Technol. Transl. Life Sci. Innov. (2019) 2472630319860775. doi:10.1177/2472630319860775.

[17] T. V. Kirk, N. Szita, Oxygen transfer characteristics of miniaturized bioreactor systems, Biotechnol. Bioeng. 110 (2013) 1005–1019. doi:10.1002/bit.24824.

[18] R. Bareither, D. Pollard, A review of advanced small-scale parallel bioreactor technology for accelerated process development: Current state and future need, Biotechnol. Prog. 27 (2011) 2–14. doi:10.1002/btpr.522.

[19] M. Tai, A. Ly, I. Leung, G. Nayar, Efficient high-throughput biological process characterization: Definitive screening design with the Ambr250 bioreactor system, Biotechnol. Prog. 31 (2015) 1388–1395. doi:10.1002/btpr.2142.

[20] A. Kusterer, Æ.C. Krause, D. Weuster-botz, Fully automated single-use stirred-tank bioreactors for parallel microbial cultivations, (2008) 207–215. doi:10.1007/s00449-007-0195-z.

[21] F. Kensy, E. Zang, C. Faulhammer, R.-K. Tan, J. Büchs, Validation of a high-throughput fermentation system based on online monitoring of biomass and fluorescence in continuously shaken microtiter plates, Microb. Cell Fact. 8 (2009) 31. doi:10.1186/1475-2859-8-31.

[22] B. Knorr, H. Schlieker, H.-P. Hohmann, D. Weuster-Botz, Scale-down and parallel operation of the riboflavin production process with *Bacillus subtilis*, Bochem. Eng. J. 33 (2007) 263–274. doi:DOI: 10.1016/j.bej.2006.10.023.

[23] A. Sawatzki, S. Hans, H. Narayanan, B. Haby, N. Krausch, M. Sokolov, F. Glauche, S.L. Riedel, P. Neubauer, M.N. Cruz Bournazou, Accelerated Bioprocess Development of Endopolygalacturonase-Production with Saccharomyces cerevisiae Using Multivariate Prediction in a 48 Mini-Bioreactor Automated Platform, Bioengineering. 5 (2018). doi:10.3390/bioengineering5040101.

[24] J. Hemmerich, N. Tenhaef, C. Steffens, J. Kappelmann, M. Weiske, S.J. Reich, W. Wiechert, M. Oldiges, S. Noack, Less Sacrifice, More Insight: Repeated Low-Volume Sampling of Microbioreactor Cultivations Enables Accelerated Deep Phenotyping of Microbial Strain Libraries, Biotechnol. J. 1800428 (2018) 1–10. doi:10.1002/biot.201800428.

[25] M.N. Cruz Bournazou, T. Barz, D.B. Nickel, D.C. Lopez Cárdenas, F. Glauche, A. Knepper, P. Neubauer, Online optimal experimental re-design in robotic parallel fed-batch cultivation facilities, Biotechnol. Bioeng. 114 (2017) 610–619. doi:10.1002/bit.26192.

[26] V. Abt, T. Barz, M.N. Cruz-Bournazou, C. Herwig, P. Kroll, J. Möller, R. Pörtner, R. Schenkendorf, Model-based tools for optimal experiments in bioprocess engineering, Curr. Opin. Chem. Eng. (2018) 244–252. doi:10.1016/j.coche.2018.11.007.

[27] M. von Stosch, M.J. Willis, Intensified design of experiments for upstream bioreactors, Eng. Life Sci. 17 (2017) 1173–1184. doi:10.1002/elsc.201600037.

[28] J. Möller, K.B. Kuchemüller, T. Steinmetz, K.S. Koopmann, R. Pörtner, Model-assisted Design of Experiments as a concept for knowledge-based bioprocess development, Bioprocess Biosyst. Eng. 42 (2019) 867–882. doi:10.1007/s00449-019-02089-7.

[29] S. Hans, C. Ulmer, H. Narayanan, T. Brautaset, N. Krausch, P. Neubauer, I. Schäffl, M. Sokolov, M.N. Cruz Bournazou, Monitoring Parallel Robotic Cultivations with Online Multivariate Analysis, Processes. 8 (2020). doi:10.3390/pr8050582.

[30] H. Narayanan, M.F. Luna, M. von Stosch, M.N. Cruz-Bournazou, G. Polotti, M. Morbidelli, A. Butté, M. Sokolov, Bioprocessing in the Digital Age: The Role of Process Models, Biotechnol. J. 15 (2020) 1900172.

doi:10.1002/biot.201900172.

[31] F. Käß, I. Hariskos, A. Michel, H.J. Brandt, R. Spann, S. Junne, W. Wiechert, P. Neubauer, M. Oldiges, Assessment of robustness against dissolved oxygen/substrate oscillations for C. glutamicum DM1933 in two-compartment bioreactor, Bioprocess Biosyst. Eng. 37 (2014) 1151–1162. doi:10.1007/s00449-013-1086-0.

[32] E. Anane, A. Sawatzki, P. Neubauer, M.N. Cruz-Bournazou, Modelling concentration gradients in fed-batch cultivations of E. coli – towards the flexible design of scale-down experiments, J. Chem. Technol. Biotechnol. 94 (2019) 516–526. doi:10.1002/jctb.5798.

[33] D.B. Nickel, M.N. Cruz-Bournazou, T. Wilms, P. Neubauer, A. Knepper, Online bioprocess data generation, analysis, and optimization for parallel fed-batch fermentations in milliliter scale, Eng. Life Sci. 17 (2017) 1195–1201. doi:10.1002/elsc.201600035.

[34] U. Sauer, D.R. Lasko, J. Fiaux, M. Hochuli, R. Glaser, T. Szyperski, K. Wüthrich, J.E. Bailey, Metabolic Flux Ratio Analysis of Genetic and Environmental Modulations of Escherichia coli Central Carbon Metabolism, J. Bacteriol. 181 (1999) 6679 LP – 6688. doi:10.1128/JB.181.21.6679-6688.1999.

[35] T. Baba, T. Ara, M. Hasegawa, Y. Takai, Y. Okumura, M. Baba, K.A. Datsenko, M. Tomita, B.L. Wanner, H. Mori, Construction of Escherichia coli K-12 in-frame, single-gene knockout mutants: the Keio collection, Mol. Syst. Biol. 2 (2006). doi:10.1038/msb4100050.

[36] E. Anane, D.C. López C, P. Neubauer, M.N. Cruz Bournazou, Modelling overflow metabolism in Escherichia coli by acetate cycling, Biochem. Eng. J. 125 (2017) 23–30. doi:10.1016/j.bej.2017.05.013.

[37] A.C. Hindmarsh, P.N. Brown, K.E. Grant, S.L. Lee, R. Serban, D.A.N.E. Shumaker, C.S. Woodward, SUNDIALS : Suite of Nonlinear and Differential / Algebraic Equation Solvers, ACM Trans. Math. Softw. 31 (2005) 363–396. doi:10.1145/1089014.1089020.

[38] D.C. López, T. Barz, M. Peñuela, A. Villegas, S. Ochoa, G. Wozny, Model-based identifiable parameter determination applied to a simultaneous saccharification and fermentation process model for bio-ethanol production, Biotechnol. Prog. 29 (2013) 1064–1082. doi:10.1002/btpr.1753.

[39] S.-O. Enfors, L. Haïggstrïom, Bioprocess Technology: Fundamentals and Applications, 2000. doi:10.1007/978-1-4613-8748-0.

[40] N. Krausch, T. Barz, A. Sawatzki, M. Gruber, S. Kamel, P. Neubauer, M.N. Cruz Bournazou, Monte Carlo Simulations for the Analysis of Non-linear Parameter Confidence Intervals in Optimal Experimental Design, Front. Bioeng. Biotechnol. 7 (2019) 122. doi:10.3389/fbioe.2019.00122.

[41] E. Anane, D.C.L. C., T. Barz, G. Sin, K. V Gernaey, P. Neubauer, M.N.C. Bournazou, Output uncertainty of dynamic growth models: effect of uncertain parameter estimates on model reliability, Biochem. Eng. J. (2019) 107247. doi:10.1016/j.bej.2019.107247.

[42] T. Barz, A. Sommer, T. Wilms, P. Neubauer, M.N.C. Bournazou, H. Throughput, Adaptive optimal operation of a parallel robotic liquid handling station, Proc. 9th Vienna Int. Conf. Math. Model. Febr. 21-23, Vienna, Austria. (2018) 901–906. doi:10.1016/j.ifacol.2018.04.006.

[43] P. Neubauer, H.Y. Lin, B. Mathiszik, Metabolic load of recombinant protein production: Inhibition of cellular capacities for glucose uptake and respiration after induction of a heterologous gene in Escherichia coli, Biotechnol. Bioeng. 83 (2003) 53–64. doi:10.1002/bit.10645.

[44] Z. Duan, M.N. Cruz Bournazou, C. Kravaris, Dynamic model reduction for two-stage anaerobic digestion processes, Chem. Eng. J. 327 (2017) 1102–1116. doi:10.1016/j.cej.2017.06.110.